ELSEVIER

Contents lists available at ScienceDirect

Optics Communications

journal homepage: www.elsevier.com/locate/optcom



Nonparaxial circular grating diffraction properties of radially polarized beams



Jiang Zhao, Bo Li, Heng Zhao, Wenjin Wang, Yi Hu, Youqing Wang*

Wuhan National Laboratory for Optoelectronics, School of Optical and Electronic Information, Huazhong University of Science and Technology, Wuhan 430074, China

ARTICLE INFO

Article history:
Received 27 September 2013
Received in revised form
16 February 2014
Accepted 22 February 2014
Available online 6 March 2014

Keywords: Radially polarized beams Nonparaxial grating diffraction Circular grating

ABSTRACT

The Rayleigh–Sommerfeld diffraction integral is employed to study the circular grating nonparaxial diffraction properties of the radially polarized beams, and the analytical expression for the diffraction electric field is derived. The analyses indicate that the properties of the nonparaxial diffraction field strongly depend on the grating parameters and beam waist. When the radially polarized beam is diffracted by the sub-wavelength grating, only the 0th diffraction ring is obtained, or the distinct higher order diffraction rings will emerge. Compared with the paraxial diffraction, the nonparaxial diffraction intensity field is weaker. But when the beam waist is larger than 3λ the paraxial approximation is valid; thus their distinction will be negligible. At last, it shows that in the radially polarized beams nonparaxial diffraction field, the longitudinal component not only leads to stronger diffraction intensity than the azimuthally polarized beams, but also makes the polarization degenerate.

© 2014 Elsevier B.V. All rights reserved.

1. Introduction

In recent decades, cylindrically vector polarized beams (CVPBs) [1] have attracted considerable research interest, owing to the peculiar spatial polarization distribution. Radially polarized beams (RPBs) and azimuthally polarized beams (APBs) are a pair of the most common orthotropic cylindrically vector polarized beams. Some potential applications for RPBs have been demonstrated, such as particle acceleration [2,3], metal cutting [4,5], photonic crystal fabrication [6], near field microscopy [7–9], particle trapping [10] and surface plasmon polariton excitation [11,12]. On the other hand, APBs are also verified to be effective in drilling [13], welding [5], split ring resonators excitation [14] and atom guiding [15]. In microscopy and particle trapping, more tiny spots, ultralong depth of the focus (DOF) or three-dimensional optical chain can be obtained by tight focusing the amplitude masks or phase plates modulated RPBs or APBs for improving the resolution or using in multi-small particles trapping [16-23]. In some of these applications, the RPBs need to pass through the multi-annual belts or grating-like optical diffraction elements. In addition, the multiple rings of the circular grating diffraction field have been used in alignment or metrology [24], which may also be the potential application for the RPBs circular grating diffraction. Therefore, the research of the nonparaxial and paraxial RPBs circular grating diffraction behaviors becomes significant in guiding these applications. To the best of our knowledge, few researches have focused on nonparaxial RPBs circular aperture [25] or annular aperture diffraction [26], and the circular grating diffraction properties of RPBs or APBs have not been reported yet. In order to figure out the nonparaxial and paraxial RPBs circular grating diffraction behaviors, the Rayleigh–Sommerfeld integrals are resolved, and the explicit diffraction electric fields are obtained in this paper. The RPBs diffracting through circular aperture and propagating in free space can be considered as two kinds of special conditions of the circular grating diffraction.

2. Grating diffraction theory of vector polarized beams

As one of the widely used vector diffraction integration theories, Rayleigh–Sommerfeld integral is demonstrated to be effective in the vector beam propagating in free space and diffracting through the circular aperture with the convergent resolutions. Here it is also used to analyze the circular grating diffraction properties of RPBs, and the diffraction scheme is shown in Fig. 1.

In the Cartesian coordinate system, the circular grating locates at the plane in z = 0. T, f and b are grating period, duty-cycle and opaque annular belt width, respectively. An aperture with radius a is in the center of the grating. The grating period number is $N(N = 1, 2, 3, 4, \cdots)$. Therefore, the grating transmission function

^{*} Corresponding author.

E-mail address: yqwang13@163.com (Y. Wang).

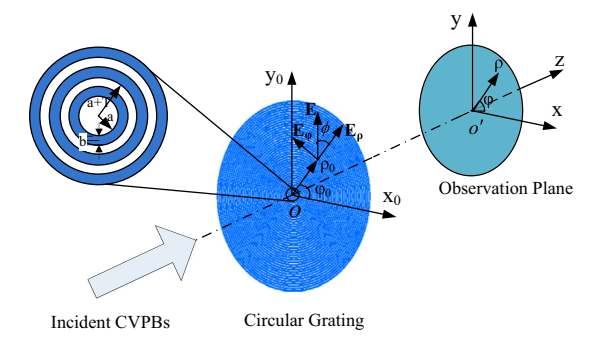


Fig. 1. The scheme of circular grating diffraction for cylindrically vector polarized beams.

can be written as

$$t(x_0, y_0) = \begin{cases} 1 & (N-1)T + a + b \le \sqrt{x_0^2 + y_0^2} < NT + a & \text{and} \quad 0 < \sqrt{x_0^2 + y_0^2} \le a \\ 0 & \text{others} \end{cases}$$
 (1)

Given the waist of incident CVPBs lies in plane z = 0, in which the transverse electric field of CVPBs can be written as

$$E(x_0, y_0, 0) = E_x(x_0, y_0, 0)\overrightarrow{e_x} + E_y(x_0, y_0, 0)\overrightarrow{e_y}$$
 (2)

$$E_{x}(x_{0}, y_{0}, 0) = \frac{\sqrt{2}E_{0}\rho_{0}}{\omega_{0}}\cos(\varphi_{0} + \phi)L_{n}^{1}\left(\frac{2\rho_{0}^{2}}{\omega_{0}^{2}}\right)\exp\left(-\frac{\rho_{0}^{2}}{\omega_{0}^{2}}\right)$$
(3)

$$E_{y}(x_{0}, y_{0}, 0) = \frac{\sqrt{2}E_{0}\rho_{0}}{\omega_{0}} \sin(\varphi_{0} + \phi)L_{n}^{1}\left(\frac{2\rho_{0}^{2}}{\omega_{0}^{2}}\right) \exp\left(-\frac{\rho_{0}^{2}}{\omega_{0}^{2}}\right)$$
(4)

where $\overrightarrow{e_x}$ and $\overrightarrow{e_y}$ are two unit vectors in x and y directions, $\rho_0 = \sqrt{x_0^2 + y_0^2}$ and $\varphi_0 = \arctan(y_0/x_0)$ are the polar radius and polar angle in grating plane, respectively, and ϕ is the angle between electric vector direction and polar radius direction. E_0 is the initial electric amplitude, ω_0 is the waist of fundamental mode CVPBs, and $L_n^1(\,\cdot\,)$ is the Laguerre polynomial in the nth order with index 1.

According to the Rayleigh–Sommerfeld integrals, the grating transmission function modulated monochromatic electric field in z>0 half-space which is filled with homogeneous medium can be expressed as

$$E_{x}(x,y,z) = -i\frac{z}{\lambda} \frac{\exp(ikr)}{r^{2}} \iint_{+\infty}^{-\infty} E_{x}(x_{0},y_{0},0) t(x_{0},y_{0},0)$$

$$\exp\left(ik\frac{x_{0}^{2} + y_{0}^{2} - 2xx_{0} - 2yy_{0}}{2r}\right) dx_{0} dy_{0}$$
(5)

$$E_{y}(x,y,z) = -i\frac{z}{\lambda} \frac{\exp(ikr)}{r^{2}} \iint_{+\infty}^{+\infty} E_{y}(x_{0},y_{0},0) t(x_{0},y_{0},0)$$

$$\exp\left(ik\frac{x_{0}^{2} + y_{0}^{2} - 2xx_{0} - 2yy_{0}}{2r}\right) dx_{0} dy_{0}$$
(6)

$$E_z(x,y,z) = i \frac{z}{\lambda} \frac{\exp(ikr)}{r^2} \iint_{+\infty}^{-\infty} [(x-x_0)E_x(x_0,y_0,0) + (y-y_0)E_y(x_0,y_0,0)]$$

$$t(x_0, y_0, 0) \exp\left(ik\frac{x_0^2 + y_0^2 - 2xx_0 - 2yy_0}{2r}\right) dx_0 dy_0 \tag{7}$$

where $t(x_0, y_0, 0)$ is the grating transmission function, k is the wave number, and $r = \sqrt{x^2 + y^2 + z^2}$.

For the CVPBs, one can substitute Eqs. (1), (3), and (4) into Eqs. (5)–(7), and transform the Cartesian coordinate system into cylindrical coordinate. Then, after tedious and direct integral, the

grating diffracted electric fields are obtained

$$\begin{split} E(x,y,z) &= -\frac{\sqrt{2}E_{0}k\exp(ikr)}{r^{2}\omega_{0}} \\ &\sum_{q=0}^{n} \sum_{m=0}^{\infty} \frac{(n+1)!(-1)^{q+m}}{(q+1)!q!(n-q)!} \frac{2^{q-1}}{\omega_{0}^{2q}} \frac{1}{g^{m+q+2}m!(m+1)!} \\ &\left\{ \sum_{N=1}^{\infty} \left[\Gamma(m+q+2,g(NT-T+a+b)^{2}) \right. \right. \\ &\left. - \Gamma(m+q+2,g(NT+a)^{2}) \right] - \Gamma(m+q+2,ga^{2}) \\ &\left. + (m+q+1)! \right\} \\ &\left\{ \left(\frac{kz\rho}{2r} \right) \frac{1}{m!(m+1)!} \left[\cos{(\varphi+\phi)} \overrightarrow{e_{x}} + \sin{(\varphi+\phi)} \overrightarrow{e_{y}} \right] \right. \\ &\left. - \left[\rho \left(\frac{k\rho}{2r} \right) \frac{1}{m!(m+1)!} - \frac{i}{m!m!} \right] \cos{\phi} \overrightarrow{e_{z}} \right\} \end{split} \tag{8}$$

where $\overrightarrow{e_z}$ is unit vector in z direction, $\rho = \sqrt{x^2 + y^2}$, $g = 1/\omega_0^2 - ik/(2r)$, and the incomplete gamma function $\Gamma(\cdot,\cdot)$. The diffraction field can be simply presented as $E_{n1} = E_x \overrightarrow{e_x} + E_y \overrightarrow{e_y} + E_z \overrightarrow{e_z}$, where E_z is the z component of the electric field. Eq. (8) indicates that the electric fields of CVPBs maintain cylindrical symmetry after being diffracted by the circular grating. In addition, the z component electric field is obtained for the RPBs (where $\phi = 0$), while there is not any z component of electric field for the APBs (where $\phi = \pi/2$). Besides, when the opaque belt width b = T and polarization vector angle $\phi = 0$, Eq. (8) reduces to Eq. (16) in Reference [25] which demonstrated the circular aperture diffraction properties of RPBs. Similarly, when the opaque belt width b = 0, and polarization vector angle $\phi = 0$, Eq. (8) reduces to Eqs. (10)–(12) in Reference [27], which presented the free space propagation properties of RPBs.

Considering the paraxial approximation, r can be expanded into Taylor series neglecting the higher order terms

$$r = z + (x^2 + y^2)/(2z) \tag{9}$$

One can substitute r of exponential part in Eq. (8) with Eq. (9) and the other terms with z. Then, the electric fields of CVPBs diffracted by circular grating under the paraxial approximation are obtained

$$\begin{split} E^{p}(x,y,z) &= -\frac{\sqrt{2}E_{0}k}{z^{2}\omega_{0}} \exp\left[ik\left(z + \frac{\rho^{2}}{2z}\right)\right] \\ &\sum_{q=0}^{n} \sum_{m=0}^{\infty} \frac{(n+1)!(-1)^{q+m}}{(q+1)!q!(n-q)!} \frac{2^{q-1}}{\omega_{0}^{2q}} \frac{1}{g_{1}^{m+q+2}} \frac{\left(\frac{k\rho}{2z}\right)^{2m}}{m!(m+1)!} \\ &\left\{ \sum_{N=1}^{\infty} \left[\Gamma(m+q+2,g_{1}(NT-T+a+b)^{2}) - \Gamma(m+q+2,g_{1}(NT+a)^{2})\right] - \Gamma(m+q+2,g_{1}a^{2}) + (m+q+1)! \right\} \\ &\left\{ \frac{k\rho}{2} \frac{1}{m!(m+1)!} \left[\cos\left(\varphi+\phi\right)\overrightarrow{e_{x}} + \sin\left(\varphi+\phi\right)\overrightarrow{e_{y}}\right] - \left[\rho\left(\frac{k\rho}{2z}\right) \frac{1}{m!(m+1)!} - \frac{i}{m!m!} \cos\left(\varphi+\phi\right)\overrightarrow{e_{z}} \right\} \end{split}$$
(10)

where $g_1 = 1/\omega_0^2 - ik/(2z)$.

3. Numerical results and discussions

Based on the derived CVPBs circular grating diffracted electric fields, the RPBs nonparaxial and paraxial diffraction behaviors are discussed in this section. In this paper, all length units are normalized by wavelength $\lambda = 1$, and the incident beam amplitude is $E_0 = 1$. As presented in previous works [25,26], the observation plane is set

at plane $z=10z_R$ in the diffraction area (z>0), where $z_R=\pi\omega_0^2/\lambda$ is the Rayleigh length. The 0th order RPBs and APBs (n=0) with beam waist $\omega_0=\lambda$ diffracted nonparaxially by a circular grating with period $T=1.5\lambda$, duty-cycle f=1-b/T=0.5and central aperture radius $a=0.3\lambda$ are calculated. The intensity field $(I=|E_x|^2+|E_y|^2+|E_z|^2)$ of the RPBs and APBs is plotted in Fig. 2(a) and (b). The two beams are of the similar diffraction patterns, namely the two concentric rings, but the diffraction rings intensity of the RPBs is slightly larger than the APB's, as shown in Fig. 2(c). This is due to the longitudinal intensity component $(|E_z|^2)$ added in RPB's diffraction intensity field except for the transverse intensity component $(|E_x|^2+|E_y|^2)$, as shown in Fig. 2(d) and (e). For longitudinal intensity component, the maximum of the 1st order diffraction intensity is almost as large as the 0th order diffraction intensity. However, the longitudinal

intensity component is still very small, compared with the 0th order diffraction transverse intensity component, as seen in Fig. 2(f). Besides, it is noteworthy that the central intensity of the longitudinal intensity component becomes nonzero.

The polarization can also be characterized by the well known Stocks parameters, even the RPB's focus field with longitudinal electrical component [28,29]. In this paper, the Stocks parameters are employed to discuss the polarization properties of the grating diffraction field. In the ρ –z plane, the radially electrical component $\overrightarrow{E}_{\rho} = \overrightarrow{E}_{x} + \overrightarrow{E}_{y}$ and longitudinal electrical component \overrightarrow{E}_{z} are considered as a pair of basic orthotropic electrical vectors in Stocks parameter, where S_{0} , S_{1} , S_{2} and S_{3} are defined as

$$S_0 = |E_z|^2 + |E_\rho|^2 \tag{11}$$

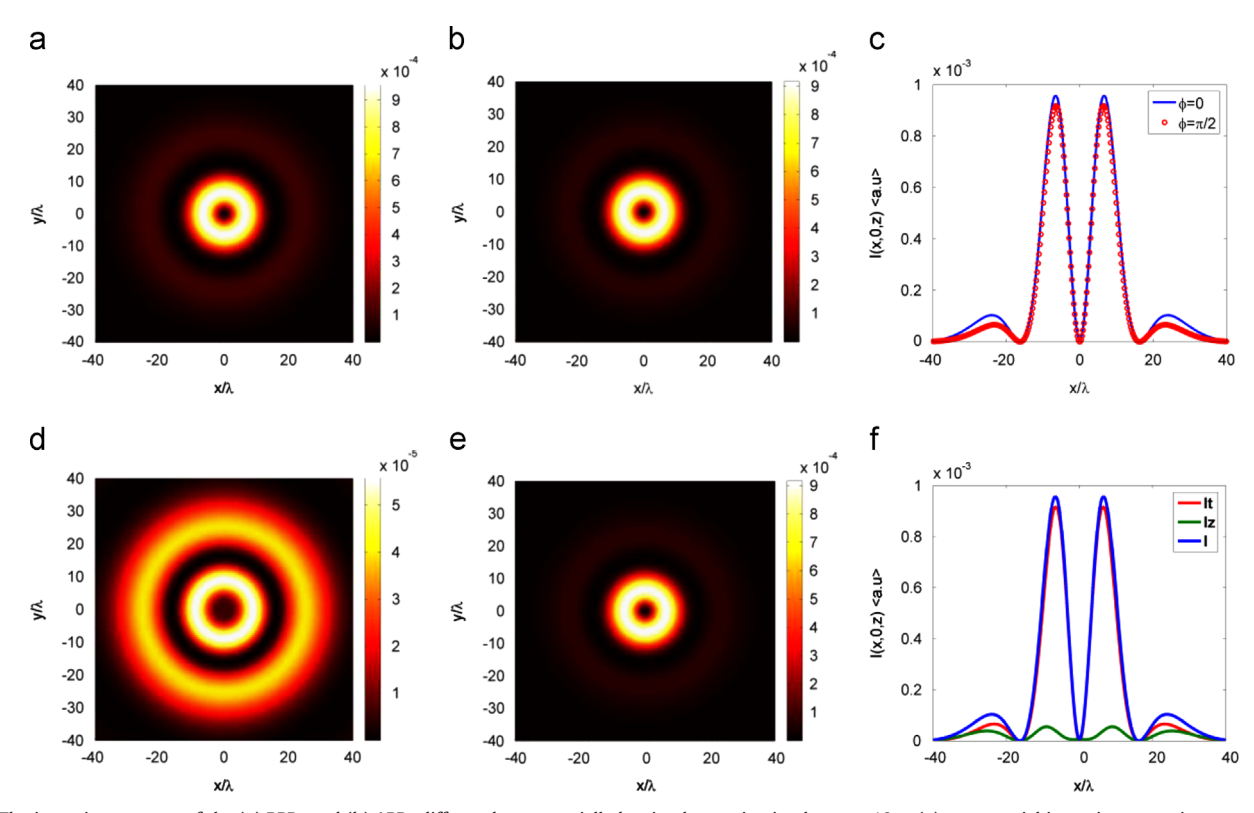


Fig. 2. The intensity contours of the (a) RPBs and (b) APBs diffracted nonparaxially by circular grating in plane $z = 10z_R$, (c) nonparaxial intensity curves in cross-section in the plane y = 0, (d) longitudinal and (e) transverse intensity component contours and (f) intensity curves of RPBs in the cross-section in plane y = 0; calculation parameters: $\omega_0 = \lambda$, n = 0, $a = 0.3\lambda$, $T = 1.5\lambda$ and f = 0.5.

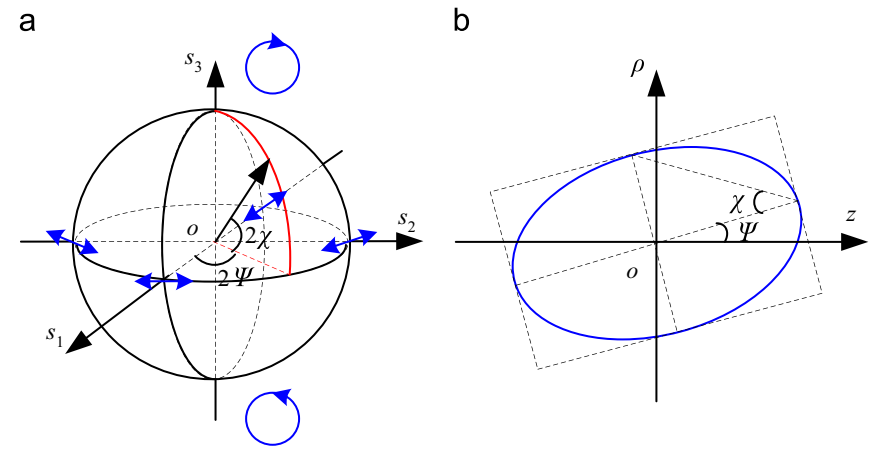


Fig. 3. (a) Schematic diagram of the Poincaré sphere and (b) the polarization ellipse.

$$S_1 = |E_z|^2 - |E_\rho|^2 \tag{12}$$

$$S_2 = 2\text{Re}\{E_2 E_{\rho}^*\}$$
 (13)

$$S_3 = -2\operatorname{Im}\{E_z E_a^*\} \tag{14}$$

For a point in the observation plane, one can get its coordinate position on the Poincaré sphere by normalizing the Stokes parameters as $s_1 = S_1/S_0$, $s_2 = S_2/S_0$ and $s_3 = S_3/S_0$. On the Poincaré sphere, each coordinate position represents a polarization state, as shown in Fig. 3. The northern and southern poles are right and left circular polarized states, respectively, while the equator means the linearly polarized state. The others represent elliptical polarized state which can be described by orientation angle, eccentricity and handedness. The orientation angle

$$\psi = \arctan(s_2/s_1)/2 \tag{15}$$

where $0 \le \psi < \pi$ is the angle between the *z*-axis and the major axis of the polarization ellipse. While the eccentricity | tan χ | represents the ratio of the two ellipse axes, where

$$\chi = \arcsin(s_3)/2 \tag{16}$$

is the ellipticity angle, $-\pi/4 \le \chi < \pi/4$. When χ is positive, the sense of handedness means right handed; otherwise, it is left handed. In the observation plane, the polarization properties of the electric field along the radial direction are studied; the orientation and ellipticity angle curves of the polarization ellipses are shown in Fig. 4. In some areas, pointed as A, B and C, both

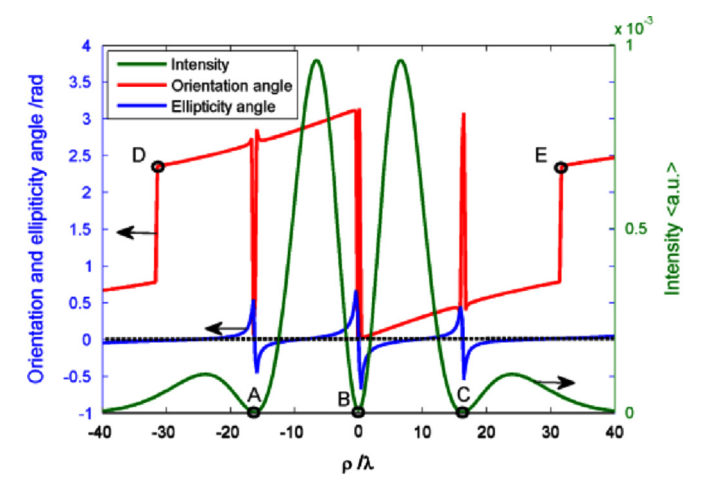


Fig. 4. The intensity, orientation and ellipticity angle curves of the circular grating diffracted RPBs, in plane $z=10z_R$; calculation parameters: $\omega_0=\lambda$, n=0, $a=0.3\lambda$, $T=1.5\lambda$ and f=0.5. (For interpretation of the references to color in this figure, the reader is referred to the web version of this article.)

the orientation and ellipticity angles are dramatically changed. However, the electric field intensities are so weak that the polarization information is not considered in these areas. For the other places, the ellipticity angle (blue line) is almost linear-like but unequal to zero, which confirms that the polarization in the ρ –z plane reduces from linear polarization to elliptical polarization due to the longitudinal component. Nevertheless, as a result of the small longitudinal component E_z , the ellipticity angle is not very large, which means that the polarization ellipse is pretty oblate. In order to distinguish the handedness, a black dot line $\gamma = 0$ is added, as shown in Fig. 4. It is clear that in each order of the diffraction field there are both the left and right hand elliptical polarization states. For the orientation angle (red line), it distributes symmetrically to the optical axis $\rho = 0$. For the two discrete points, shown as D and E, where the transverse component equals the longitudinal component (seen in Fig. 2(f)), which means that Stocks parameter S_1 is 0, mathematically, ψ can be either $\pi/4$ or $-\pi/4$. Therefore, when the orientation angle ψ is negative, according to the definition, π is added for keeping it positive.

The paraxial and nonparaxial RPBs circular grating diffraction properties of the different orders are also studied. As shown in Fig. 5(a)-(c), the paraxial diffraction effect is stronger than the nonparaxial diffraction's, and there are not only the 0th and 1st order diffraction rings but also the 2nd order ring. Moreover, for each nonparaxial diffraction order, the maximum intensity is also weaker than the paraxial diffraction's. To the higher order RPBs, as much more diffraction rings arise, the nonparaxial and paraxial grating diffraction fields become much complex, as shown in Fig. 6. Interestingly, with the RPBs order increasing, more and more nonparxial and paraxial diffraction orders which locate from the diffraction pattern center to periphery tend to overlap. For example, the 0th nonparaxial and paraxial diffraction rings in Fig. 6(a), similarly, the 0th and the 1st nonparaxial and paraxial diffraction rings in Fig. 6(b) are almost overlapped. This suggests that for the wider incident beam width, the paraxial diffraction approximation is valid to calculate the intensity field distribution around the optical axis areas.

As mentioned above, the beam orders imply that the incident beam width will influence the diffraction intensity distribution. In this section the impact of the beam waist on the diffraction field will be further discussed. Here the calculation plane is fixed in $z=10\pi/\lambda$ to avoid the change in observation plane with the waist adjustment. Taking the 0th RPB's circular grating nonparaxial diffraction as example, one can easily find that the wider waist leads to the larger diffraction intensity, as shown in Fig. 7(a). This is because the bigger waist means larger grating areas illuminated by the incident beam; hence much more energy flow can pass through the grating. To further study the impact of beam waist on the circular grating diffraction field, the 0th order nonparaxial and

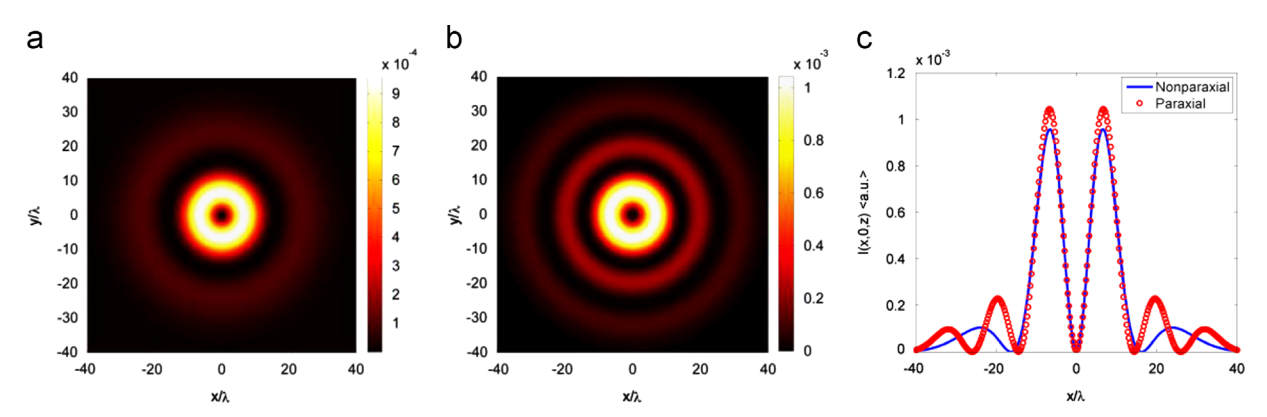


Fig. 5. The (a) nonparaxial and (b) paraxial diffraction intensity contours of the 0th order RPBs in the plane $z = 10z_R$ and (c) nonparaxial and paraxial diffraction intensity curves in the cross-section in plane y = 0; calculation parameters: $\omega_0 = \lambda$, n = 0, $a = 0.3\lambda$, $T = 1.5\lambda$, and f = 0.5.

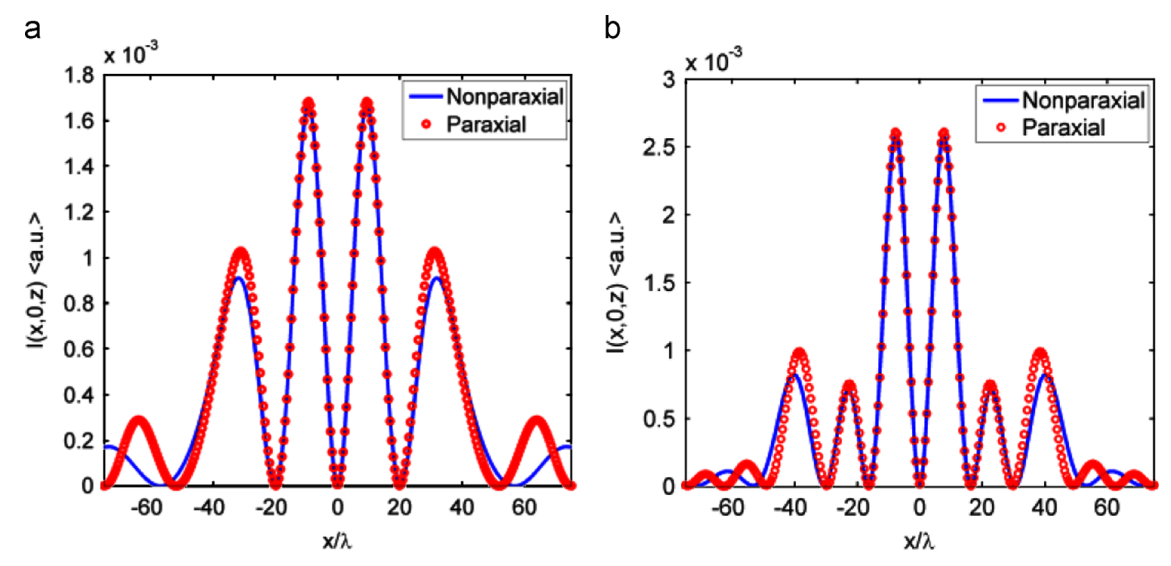


Fig. 6. The nonparaxial and paraxial diffraction intensity curves of (a) the 1st order n = 1, and (b) the 2nd order n = 2 RPBs in the cross-section in plane $z = 10z_R$; calculation parameters: $\omega_0 = \lambda$, $a = 0.3\lambda$, $T = 1.5\lambda$, and f = 0.5.

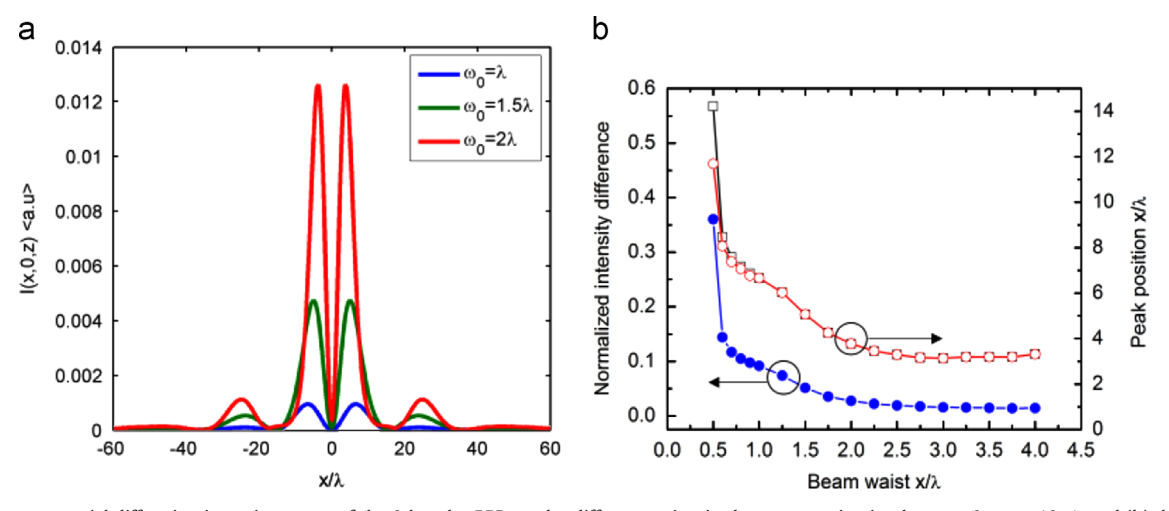


Fig. 7. (a) The nonparaxial diffraction intensity curves of the 0th order RPBs under different waists in the cross-section in plane y = 0 at $z = 10\pi/\lambda$ and (b) the normalized intensity difference of the 0th order diffraction peaks (blue dots line), the 0th order nonparaxial (red circle line) and paraxial (black square line) diffraction peak positions versus the beam waist calculation parameters: n = 0, $a = 0.3\lambda$, $T = 1.5\lambda$, and f = 0.5. (For interpretation of the references to color in this figure legend, the reader is referred to the web version of this article.)

paraxial diffraction peak positions and normalized intensity difference are studied. The normalized intensity difference is defined as $\beta = |I^n - I^p|/I^n$, where I^n and I^p are the 0th order nonparaxial and paraxial diffraction peak intensities, respectively. As plotted in Fig. 7(b), the normalized intensity difference (blue dots line) decreases with increasing waist. When the beam waist reaches to 3λ , the normalized intensity difference reduces to 1.57%. This implies that the intensity difference between the nonparaxial and paraxial circular grating diffractions can be neglected and the paraxial approximation is applicable, which is similar to the RPBs circular aperture diffraction [25]. This result is also confirmed by the 0th order diffraction peak position. It is shown that the 0th order nonparaxial (red circle line) and paraxial (black square line) diffraction peak positions gradually overlap and shift toward optical axis as the waist increases. Therefore, the RPBs nonparaxial circular grating diffraction properties can be observed under the condition that the beam waist is very small.

Besides the beam waist, a circular grating structure such as the grating period, duty-cycle and central aperture radius also plays a very important role in the diffraction intensity distribution. Therein, the grating period is also thought to be connected with

the number of diffraction order controlling. As shown in Fig. 8, the higher diffraction orders arise under the condition of bigger grating period. For example, when the grating period is 2λ , the second diffraction order is obtained. When the grating period decreases, the number of diffraction orders reduces and each of the diffraction peak deviates from optical axis. With the change in grating period, the intensity fluctuation or perturbation of each order diffraction peak occurs. This phenomenon may result from the incident RPBs peak electric field intensity alignment to the grating transmission annular periodically. Another noteworthy feature is that there is only the 0th order diffraction intensity for the sub-wavelength grating diffraction which is similar to the surface relief grating's.

In addition, the grating duty-cycle is essential for the diffraction intensity distribution, as shown in Fig. 9(a); the larger duty-cycle leads to the greater 0th order diffraction intensity. Obviously, the wider transmission annular ring allows more beam electric current to pass through the grating to the observation plane. However, when the duty-cycle is pretty large, the grating diffraction intensity becomes weak, as shown by the blue square line in Fig. 9 (b), and the ratio of the 1st order diffraction peak to the 0th order

diffraction peak decreases. Thus, one can allocate the intensity of the 0th and the 1st order diffraction rings by changing the grating duty-cycle. But it must be pointed that the position of the two orders diffraction peaks may slightly shift, when the grating duty-cycle modifies, as plotted in Fig. 9(b). Comparatively, the 0th order diffraction peak position (red triangle line) has lesser influence than the 1st order's (black triangle line).

At last, the impact of the central aperture radius a on the 0th RPBs nonparaxial diffraction intensity is discussed. When the aperture radius is very small, the incident beam waist is so large that it makes the doughnut beam mainly illuminate at the grating rings area; taking $a=0.3\lambda$ for example, the circular grating plays a prominent role in the diffraction intensity distribution with the obvious 1st order diffraction peak, as indicated by the pink curve in Fig. 10. While increasing the aperture radius a, the doughnut beam gradually covers the aperture, so the diffraction intensity distribution is impacted by the aperture more strongly. Until the

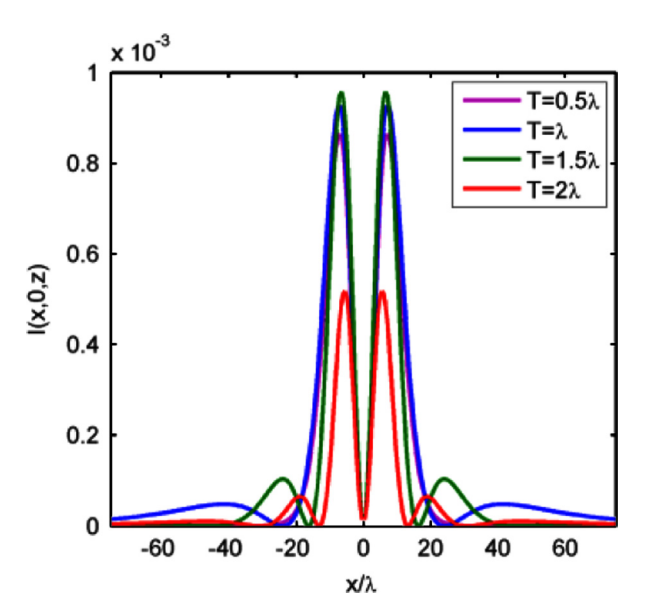


Fig. 8. The nonparaxial diffraction intensity curves of the 0th order RPBs under different grating periods in the cross-section in plane y=0, at $z=10z_R$; calculation parameters: $\omega_0=\lambda$, n=0, $a=0.3\lambda$, and f=0.5.

aperture radius reaches to 1.4λ , the diffraction intensity (red line) almost coincides with the intensity of the circular aperture diffraction (black line). In this process, the 1st order diffraction intensity gradually merges with the 0th order diffraction's, and the 0th order diffraction intensity fluctuation is also inevitable, since the transmission changes with the variation in the central aperture radius.

4. Conclusion

In summary, the nonparaxial and paraxial circular grating diffraction properties of the RPBs have been studied. The analytical expressions for the diffraction electric field have been derived based on the Rayleigh–Sommerfeld diffraction integral. The RPBs diffracted by circular aperture and propagated in free space can be considered as two kinds of special cases for the circular grating

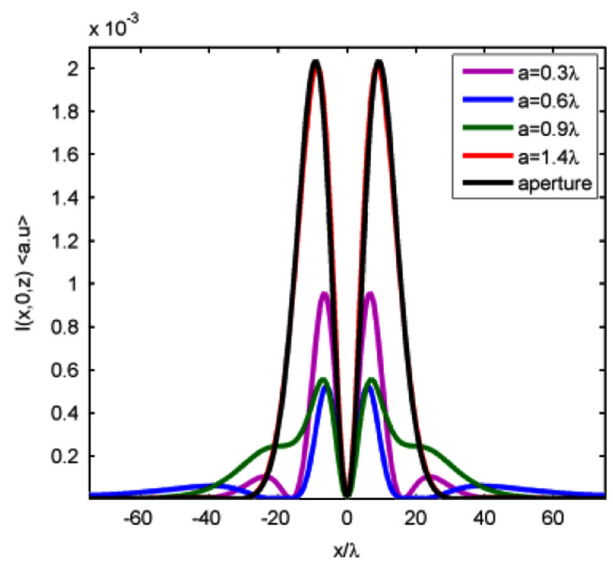


Fig. 10. The nonparaxial 0th order RPBs diffraction intensity distribution with different central aperture radii and the circular aperture diffraction with aperture radius $a = 1.4\lambda$ (black line) in the cross-section in planey = 0 at $z = 10z_R$; calculation parameters: $\omega_0 = \lambda$, n = 0, $T = 1.5\lambda$, and f = 0.5. (For interpretation of the references to color in this figure, the reader is referred to the web version of this article.)

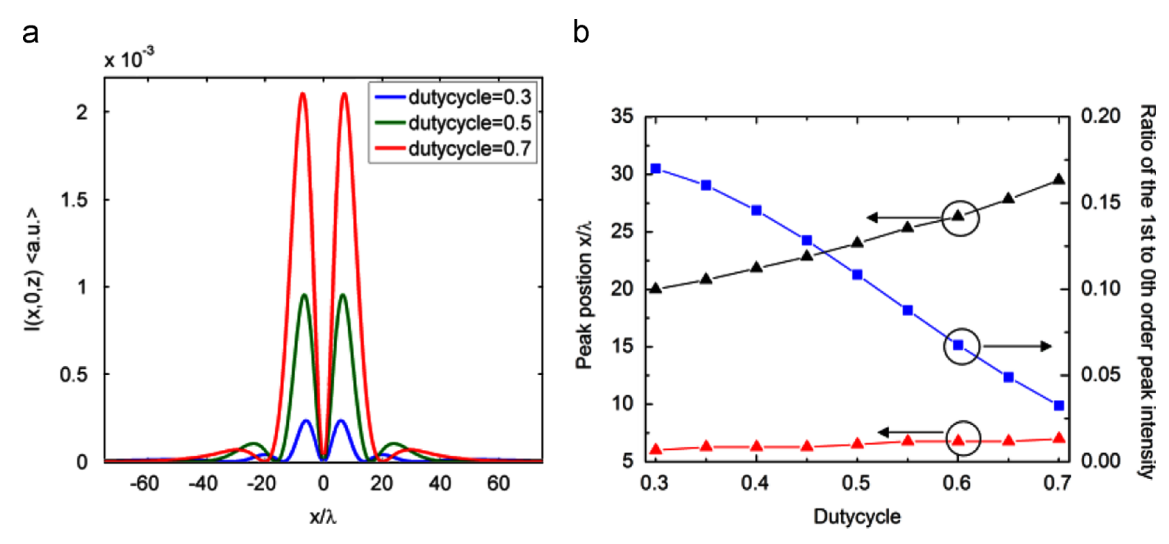


Fig. 9. (a) The nonparaxial diffraction intensity curves of the 0th order RPBs with different grating duty-cycles in the cross-section in plane y=0 at $z=10z_R$ and (b) the ratio of the 1st to 0th order diffraction peaks (blue square line), the 0th order diffraction peak (red triangle line) and the 1st diffraction peak position (black triangle line) versus the grating duty-cycle calculation parameters: $\omega_0 = \lambda$, n=0, $a=0.3\lambda$, and $T=1.5\lambda$. (For interpretation of the references to color in this figure legend, the reader is referred to the web version of this article.)

diffraction. The numerical results show that the beam waist, grating period, duty-cycle and central aperture radius play critical roles in the diffraction field. Some higher order diffraction rings exist in the nonparaxial diffraction field, except for the subwavelength circular grating diffraction. Moreover, the grating duty-cycle can be used to modify the higher diffraction intensity. Compared with the APBs, the longitudinal field component arises in RPBs circular grating diffraction, leading to the polarization degeneration from linear to elliptical in the ρ -z plane. However, the longitudinal field component is much smaller than the transverse field component especially for the large beam waist; under this circumstance, the longitudinal field component can be neglected and the nonparaxial diffraction can be approximated by the paraxial diffraction.

Acknowledgments

This work is supported by the National Natural Science Foundation of China for Young Scholars (No. 61308045).

References

- [1] O. Zhan, Adv. Opt. Photonics 1 (2009) 1.
- [2] W.D. Kimura, G.H. Kim, R.D. Romea, L.C. Steinhauer, Phys. Rev. Lett. 74 (1995) 546.
- [3] D.N. Gupta, N. Kant, D.E. Kim, H. Suk, Phys. Lett. 368 (2007) 402.

- [4] V.G. Niziev, A.V. Nesterov, J. Phys. D: Appl. Phys. 32 (1999) 1455.
- [5] R. Weber, A. Michalowski, M.A. Ahmed, V. Onuseit, V. Rominger, M. Kraus, T. Graf, Phys. Proc. 12 (2011) 21.
- [6] B. Jia, H. Kang, J. Li, M. Gu, Opt. Lett. 34 (2009) 1918.
- K.S. Youngworth, T.G. Brown, Proc. SPIE 3919 (2000) 75.
- [8] N. Hayazawa, Y. Saito, S. Kavata, Appl. Phys. Lett. 85 (2004) 6239.
- [9] W. Chen, Q. Zhan, Opt. Express 15 (2007) 4106.
- [10] Q. Zhan, Opt. Express 12 (2004) 3377.
- [11] Q. Zhan, Opt. Lett. 31 (2006) 1726.
- [12] G.M. Lerman, A. Yanai, N. Ben-Yosef, U. Levy, Opt. Express 18 (2010) 10871.
- [13] M. Meier, V. Romano, T. Feurer, Appl. Phys. A 86 (2007) 329.
- [14] J. Scheuer, Opt. Express 19 (2011) 25454.
- [15] F.K. Fatemi, M. Bashkansky, E. Oh, D. Park, Opt. Express 18 (2010) 323.
- [16] H. Lin, B. Jia, M. Gu, Opt. Lett. 36 (2011) 2471.
- [17] Y.-J. Yoon, W.-C. Kim, N.-C. Park, K.-S. Park, Y.-P. Park, Opt. Lett. 34 (2009) 1961.
- [18] L. Yang, X. Xie, S. Wang, J. Zhou, Opt. Lett. 38 (2013) 1331.
- [19] J. Lin, K. Yin, Y. Li, J. Tan, Opt. Lett. 36 (2011) 1185.
- [20] H. Wang, L. Shi, B. Lukyanchuk, C. Sheppard, C.T. Chong, Nat. Photonics 2 (2008) 501
- [21] G.H. Yuan, S.B. Wei, X.-C. Yuan, Opt. Lett. 36 (2011) 3479.
- [22] Y. Zhao, Q. Zhan, Y. Zhang, Y.P. Li, Opt. Lett. 30 (2005) 848.[23] X. Hao, C. Kuang, T. Wang, X. Liu, Opt. Lett. 35 (2010) 3928.

- [24] J. Dyson, Proc. R. Soc. A 248 (1958) 93.[25] X. Jia, Y. Wang, B. Li, Opt. Express 18 (2010) 7064.
- [26] Chen Jian-Nong, Chin. Phys. Lett. 28 (2011) 124202.
- [27] D. Deng, J. Opt. Soc. Am. B 23 (2006) 1228.
- [28] R.W. Schoonover, T.D. Visser, Opt. Express 14 (2006) 5733.
- [29] X. Pang, T.D. Visser, Opt. Express 21 (2013) 8331.